

Review

Research Progress on Metal–Organic Framework-Based Electrode Materials for Supercapacitors

Yin Zhu ^{1,2}, Peng Su ², Jiemin Wang ^{1,*}  and Xu Wang ^{2,*}¹ College of Biomedical Engineering, Sichuan University, Chengdu 610064, China; 13086655062@163.com² School of New Energy and Materials, Southwest Petroleum University, Chengdu 610500, China; chen081597@163.com

* Correspondence: jiemin@scu.edu.cn (J.W.); wwxx1969@163.com (X.W.)

Abstract: Supercapacitors play an important role in power systems since they are a key part of electrochemical energy storage devices. To assemble high-performance supercapacitors, it is crucial to discover and innovate high-capacitive electrode materials. Recently, metal–organic frameworks (MOFs) and their derivatives have received wide concerns as electrode materials for supercapacitors, not only because of their high pore volume and large surface area for ions and electrons insertion and transportation, but also due to the intrinsic metal active sites that possibly offer extra faradaic pseudocapacitance. Additionally, the abundant species of MOFs with various morphologies also feature advantages in enriching the structural diversity of electrodes. In this paper, we first report the latest research progress and demonstrate the feasibility of pure MOFs for directly constructing supercapacitor electrodes. Furthermore, different MOF derivatives, including porous carbons, transition metal oxides, metal hydroxides and MOF composites for supercapacitors, are summarized, and their electrochemical performances with corresponding energy storage mechanisms are presented in detail. Finally, the perspectives for MOF-based materials applied in supercapacitors are discussed, aiming to provide a guideline for further research based on these promising materials.

Keywords: metal–organic frameworks; derivatives; supercapacitors; energy devices; composites



Citation: Zhu, Y.; Su, P.; Wang, J.; Wang, X. Research Progress on Metal–Organic Framework-Based Electrode Materials for Supercapacitors. *Crystals* **2023**, *13*, 1593. <https://doi.org/10.3390/cryst13111593>

Academic Editor: Volodymyr Bon

Received: 11 October 2023

Revised: 7 November 2023

Accepted: 10 November 2023

Published: 17 November 2023



Copyright: © 2023 by the authors. Licensee MDPI, Basel, Switzerland. This article is an open access article distributed under the terms and conditions of the Creative Commons Attribution (CC BY) license (<https://creativecommons.org/licenses/by/4.0/>).

1. Introduction

With the exploitation of nonrenewable resources like coal, natural gas, and oil, the increasing consumption of traditional energy sources has unavoidably caused serious environmental pollution. Therefore, developing renewable and clean energy is urgent [1–4]. Nowadays, there are numerous energy conversion and storage technologies, including batteries, capacitors and nanogenerators, etc., created to hopefully replace traditional energy systems [5–8]. Among them, supercapacitors (SCs) are one of the most promising power units, because of the high-power density, quick charging and discharging ability, ease of processing, high safety and low cost. However, ordinary SCs composed of carbon materials with electrical double-layer capacitance (EDLC) deliver a relatively low energy density. This may be due to the intrinsic nature of electrode materials, where electrochemical redox for additional capacitance is normally limited [9–12]. To address this issue, many efforts have been devoted to seeking new electrode materials over the past few decades. Nevertheless, for some noncarbon materials, such as metal oxides or hydroxides, increasing the faradaic pseudocapacitance compromises other properties, such as cyclicity or stability. Therefore, the design of SC electrode materials that present excellent comprehensive performance is still challenging [13,14].

Metal–organic frameworks (MOFs) with unique physicochemical properties built by metal centers and organic ligands have recently attracted enormous attention for their energy storage and conversion capabilities. Their regular topology, high pore volume, large specific surface area, and adjustable pore size feature advantages in ion insertion and

transportation [15–19]. More importantly, the metal sites in MOFs often assist the formation of pseudocapacitance during redox reaction [17], where there is a protonation process between metal ions and electrolytes. Additionally, in some cases, the MOFs with metal nodes, such as Cu^{2+} ($3d^9$), and redox active ligands, such as benzoquinonyl, are efficient for increasing carriers' mobility, which greatly benefits the promotion of conductivity for supercapacitors [18]. Of course, the stability of pure MOFs as electrodes is also controversial, since the electrolyte anions chelating with metal ions may lead to the deconstruction of the original coordinated framework. Hence, instead of Pure MOFs, their derivatives are preferred for energy electrochemical applications. For instance, MOF crystals with a polyhedra shape are utilized as ideal precursors to construct various nanostructured carbon/metal oxide hybrids [19]. Apart from pseudocapacitance supplied by metal oxide nanoparticles, the carbonized architectures serving as EDLC further improve conductivity and stability. Nevertheless, every coin has two sides. High-temperature thermal treatment of MOFs, along with organic linkers breakage and metal cluster aggregation, sometimes gives rise to pore vanish and structural collapse, probably reversing the capacitive performances [20].

Thus, this review systematically outlines and compares the latest research progress of MOF-based materials involving pure MOFs, MOF derivatives and MOF composites for SCs, aiming to seek the optimal cases as electrode materials (Figure 1). Meanwhile, the behind energy storage mechanisms in SCs are discussed to inspire new ideas for the design of novel MOFs and their derivatives in the domain of capacitors and other power systems.

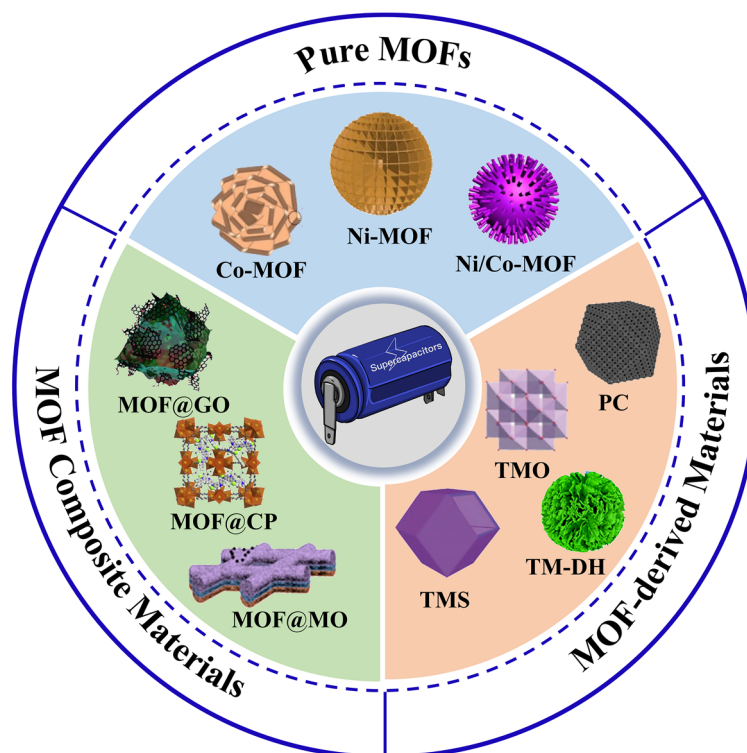


Figure 1. An illustration of several MOFs and materials for supercapacitors' electrodes that are derived from MOFs, (three types of electrode materials: Pure MOFs, MOF-derived materials, MOF composite materials). (PC: porous carbon; TMO: transition metal oxide; TM-DH: transition metal hydroxide; TMS: transition metal sulfide; CP: conductive polymer).

2. Classification of Supercapacitors

Based on their energy storage mechanisms, SCs can be divided into three categories (Figure 2): electric double-layer capacitors (EDLCs), pseudocapacitors (PCs), and hybrid capacitors (HCs) [20]. The EDLC is a Helmholtz bilayer structure formed by adsorbing ions on the surface of materials to store electric charges. EDLCs have excellent cyclic

stability while their energy density is low [21,22]. The PC generates greater capacitance through Faraday redox reaction. However, its cycle stability and energy density are both low [23,24]. HCs are generally composed of EDLCs and PCs, which can simultaneously achieve high energy density and high power density. For the selection of several types of SC electrode material, EDLCs prefer carbon-based materials such as carbon nanotubes (CNTs), graphene, and activated carbon (AC). PCs generally adapt to conductive polymers, transition metal hydroxides, and transition metal oxides (TMOs) [25–27]. Also, based on the various materials used for the positive and negative electrodes, SCs can be further categorized into symmetric SCs and asymmetric SCs [4]. Unlike symmetric SCs, asymmetric SCs feature different positive electrode and negative electrode materials, which express higher energy density and specific capacitance [28].

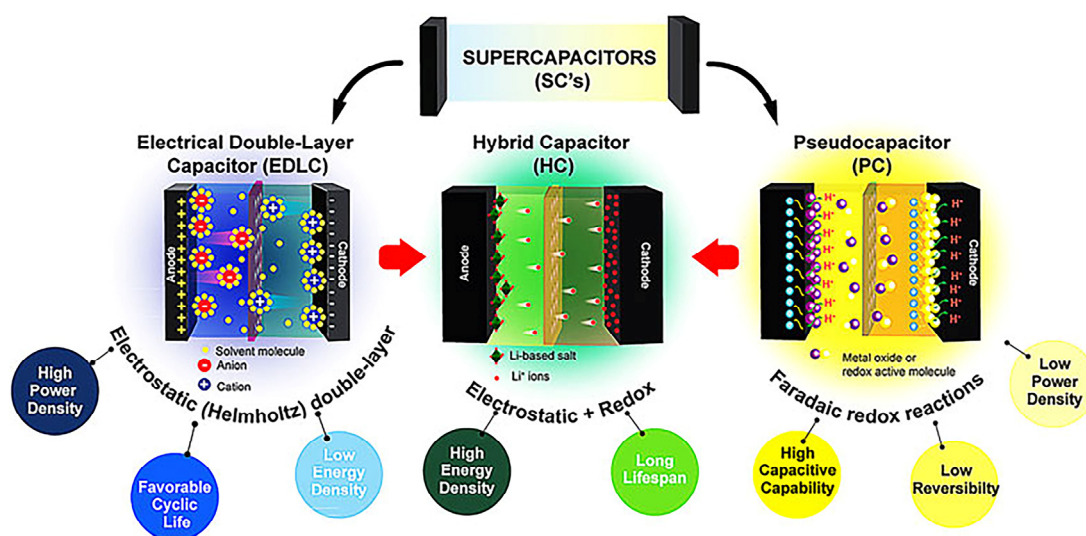


Figure 2. Schematic illustration of three categories of supercapacitors: EDLC, PC, and HC. Reproduced with permission from ref. [20]. Copyright 2021, Frontiers Media S.A.

MOFs are regarded as potential materials for novel energy storage devices because of their exceptional performance and structure. However, the low conductivity and relatively low chemical/structural stability of most original MOFs sometimes limit their application in the field of energy storage. Now, MOFs applied for SCs include pure MOFs, MOF derivatives, and MOF-based composites or hybrids.

3. Pure MOF Materials

So far, there have been many pure M-MOFs ($M = \text{Co}, \text{Ni}, \text{Zn}, \text{Mo}, \text{Fe}$) for SCs. The electrochemical performance of pure MOFs is highly dependent on their composition and structure. Additionally, the ions and electrons are affected by their pore channels. Among all the pure MOFs, Co- and Ni-based MOFs are the most-reported.

The exploration of Co-MOF for SCs was first reported by Díaz et al. [29] In 2012, they synthesized Co8-MOF-5, modified from MOF-5, where some Zn node was replaced by Co node (Figure 3a). Although Co-O redox was introduced, it still behaved like EDLCs, owing to the low conductivity. Then, in 2016, Liu et al. [30] investigated Co-based multilayer MOF (Co-LMOF) as an electrode material for SCs (Figure 3b). It delivered a high specific capacitance of 2474 F g^{-1} at a current density of 1 A g^{-1} (Figure 3c). The high capacity is attributed to the PCs. Also, it was stable even after 2000 cycles with 94.3 % capacity retaining (Figure 3d). Subsequently, Yang et al. [31] synthesized a thin nanosheet with a layered structure of Co-MOF (Figure 3e). The specific capacitance of the Co-MOF nanosheet was 2564 F g^{-1} at 1 A g^{-1} and could preserve 95.8% of its initial value after 3000 cycles (Figure 3g). This exceptional electrochemical performance is mainly ascribed to the two-dimensional (2D) layered structure with reduced dimensionality. Moreover, Ramachandran et al. [32] studied

the capacitance of the same crystal-structured Co-BTC synthesized by different conditions (Figure 3h). They found that the capacitance of as-obtained Co-MOFs differed, even under the metal/ligand connection yet different synthesis conditions. Among them, the specific capacitance of Co-MOF/D-E synthesized in DMF/EtOH delivered the maximum specific capacitance 958.1 F g^{-1} at 2 A g^{-1} , mainly ascribed to the highest deprotonation rate in that solvent system, where the rapid grown crystal showed fewer defects. Furthermore, Zhang et al. [33] continually developed Co-BTC (CBNWM) nanowire microspheres (Figure 3i). For one thing, the hierarchical superstructure enabled the enhancement of capacitance. For another, the mechanical and chemical stability of Co-MOFs were improved, thus being beneficial as electrodes for SCs. Inspired by that, Wang et al. [34] prepared a series of Co-MOF-74 microflowers through a solvent regulation strategy (Figure 3j). They found that regular and uniform Co-MOF microflowers can offer additional sites and pathways for ion and electron transfer at the interface, hence accelerating reversible redox kinetics and achieving high PCs.

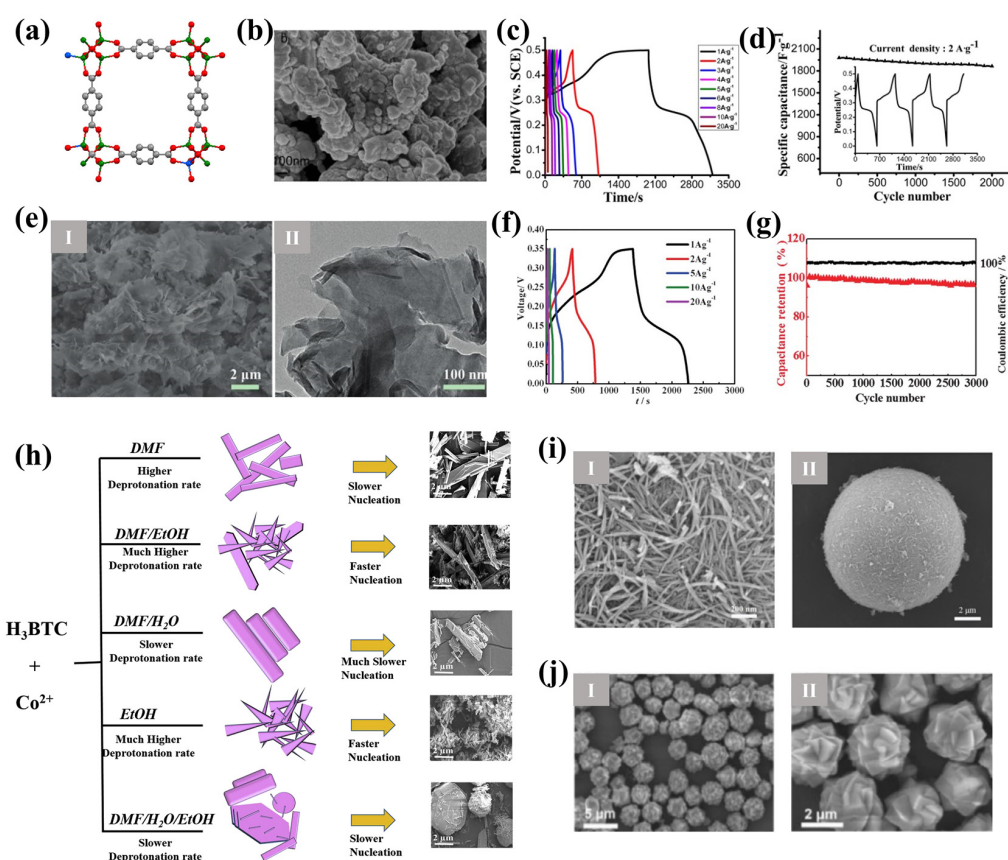


Figure 3. (a) Structural Chart of Co₈-MOF-5. Zn: green, Co: blue, C: gray, O: red. Reproduced with permission from ref. [29]. Copyright 2011 Elsevier. (b) SEM image of Co-LMOF after grinding. (c) The charge–discharge curves of the Co-LMOF electrode at different current densities. (d) Cycling performance of the Co-LMOF electrode in the potential range of 0–0.5 V at 2 A g^{-1} . The inset is a galvanostatic charge–discharge process. Reproduced with permission from ref. [30]. Copyright 2016 American Chemical Society. (e) SEM and HRTEM images of the Co-MOF material. (f) Charge–discharge profiles of the Co-MOF electrode. (g) Charge–discharge profile (black line) and specific capacitance (red line) at a current density of 2 A g^{-1} of the Co-MOF electrode. Reproduced with permission from ref. [31]. Copyright 2017 Wiley-VCH. (h) Formation mechanism of Co-MOFs in different solvents. Reproduced with permission from ref. [32]. Copyright 2018 Elsevier. (i) SEM image of CBNWN. Reproduced with permission from ref. [33]. Copyright 2021 Elsevier. (j) SEM images of Co-MOF-74 microflower. Reproduced with permission from ref. [34]. Copyright 2021 Published by Elsevier.

In addition to Co-MOFs, Ni-MOFs are also extensively reported for SC electrodes, since their specific capacitance is normally higher than CO-MOFs (Table A1). For example, Jiao et al. [35] developed a Ni-based metal–organic skeleton to improve the electrochemical performance of alkaline battery supercapacitor hybrid devices (ABSHDs) (Figure 4a). It disclosed a synergistic effect between Ni-MOF and $\text{Fe}(\text{CN})_6^{4-}/\text{Fe}(\text{CN})_6^{3-}$, where $\text{Fe}(\text{CN})_6^{4-}/\text{Fe}(\text{CN})_6^{3-}$ functioned as an electronic relay during the charging and discharging process of Ni-MOF via Ni(II)/Ni(III) transition. Meanwhile, the 2D-layered structure of Ni-MOF provided a large area for efficient charge transfer and storage. Moreover, they also fabricated asymmetric SCs: Ni-MOF/CNTs-COOH ABSHD with a power density of up to 7000 W/Kg and an energy density of 55.8 Wh/Kg. Likewise, Yan et al. [36] reported an accordion-like Ni-MOF (Figure 4b), which presented a specific capacitance of 988 F g^{-1} at 1.4 A g^{-1} . It thus highlighted the advantages of a layered structure for SC electrodes. Furthermore, Du et al. [37] adopted trimethyl acid as an organic ligand and nickel salts as metal nodes to generate a 2D Ni-MOF hierarchical structure. (Figure 4c,d). Similar to a Co-MOF superstructure, it also revealed a high specific capacitance: 1057 F g^{-1} at 1 A g^{-1} , in contrast with single-layered Ni-MOF. The architecture enabled better stability with 63.4% capacitance attained at a large current density of 30 A g^{-1} and good cyclic stability after 2500 cycles at 10 A g^{-1} . Shen and colleagues then investigated the impact of solvothermal temperature on the morphology and electrochemical properties of Ni-MOF superstructures [38]. They suggested 80°C -synthesized Ni-MOFs can form hexagonal superstructures with Ni-MOF nanofibers crossing (Figure 4e). The morphology expressed a higher surface area, thus contributing to maximum capacitance with 30.89 mAh g^{-1} at 1 A g^{-1} .

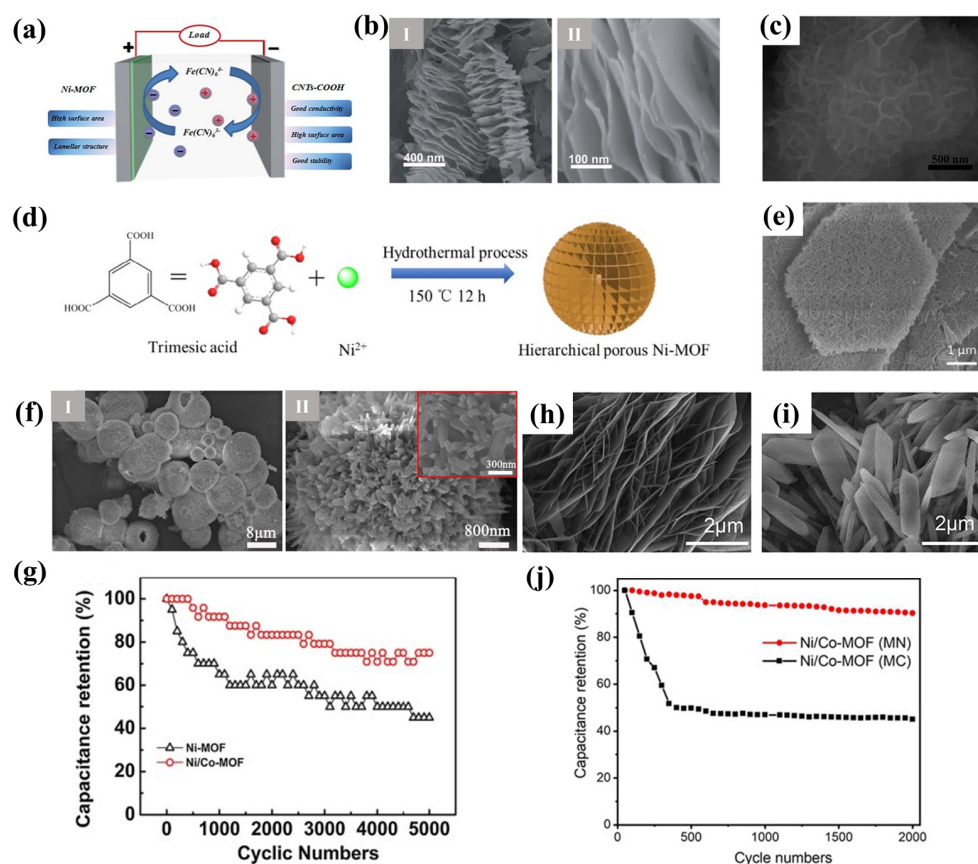


Figure 4. (a) Schematic illustration of the ABSHD cell containing Ni-MOF and CNTs-COOH as positive and negative electrodes, respectively. Reproduced with permission from ref. [35]. Copyright 2016 The Royal Society of Chemistry. (b) SEM image of the accordion-like Ni-MOF. Reproduced with permission from ref. [36]. Copyright 2016 The Royal Society of Chemistry. (c) SEM images of Ni-MOF.

(d) A schematic illustration of the fabrication process of hierarchical porous Ni-MOF. Reproduced with permission from ref. [37]. Copyright 2018 Elsevier. (e) SEM image of Ni-MOF-80. Reproduced with permission from ref. [38]. Copyright 2022 MDPI. (f) SEM images of Ni/Co-MOF. (g) Cycling performance of Ni-MOF and Ni/Co-MOF. Reproduced with permission from ref. [39]. Copyright 2018 Elsevier. (h) SEM images of MN. (i) SEM images of MC. (j) Cycling performances of MN and MC at 20 mV/s. Reproduced with permission from ref. [40]. Copyright 2022 American Chemical Society.

Except for single-metal component MOFs, multimetal MOFs are also investigated for SC electrodes. For example, Gao et al. [39] prepared Ni/Co-MOF by using Ni^{2+} and Co^{2+} (mole ratio Ni:Co = 1:1) and pyromellitic acid as an organic ligand (Figure 4f). Interestingly, compared with Ni-MOF, binary Ni/Co-MOF attained 75% of its original specific capacitance i.e., up to 758 F g^{-1} after 5000 cycles (Figure 4g), which confirmed the stability by introducing another metal component. Moreover, due to the dandelion-like morphology of the synthesized Ni/Co-MOF, it has a very rich pore structure and chemical reaction active sites. Then, to further investigate how the morphology and composition affected the electrochemical efficiency of Ni/Co-MOFs, Xu et al. [40] chose nitrate (MN) and chloride (MC) as regulators, respectively, to induce the growth of Ni/Co-MOF. Obviously, MN-regulated Ni/Co-MOF exhibited a thinner layered structure in contrast with the MC-regulated case (Figure 4h,i). As a result, the electrochemical behavior differed where Ni/Co-MOFs (MN) displayed larger capacitance and were more stable after 2000 cycles (Figure 4j). Therefore, it reflected that, for Ni, Co-constituting MOFs, the effect of morphology dominates more than ligands, where lower dimensionality brings about both improved capacitance capacity and stability.

4. MOF-Derived Materials

In addition to being directly used for SC electrode materials, MOFs can also be served as templates or precursors to evolve different electrode materials, such as porous carbon materials, transition metal oxides, metal hydroxides, and other materials. They allow for tailoring fascinating structures, enhancing intrinsic conductance, and enriching active sites to boost the capacitance to a large extent [41–43].

4.1. Porous Carbon Materials

Porous carbon materials are promising for SC electrodes because of their high conductance, hierarchical structure, large surface area and rich porosity [44,45]. So far, many methods have been employed to design porous carbon materials. Among them, high-temperature pyrolysis or carbonization from an organic precursor is the most widely utilized. Especially, to fabricate carbon materials by setting MOFs as precursors feature many profits, including ease of fabrication, polyhedron shape-inheriting, porous structure-formation, and self-doping heteroatoms (N, O and metal atoms), etc. For example, Yamauchi's team has recently reported a series of ZIF-8-derived nanoporous carbons (NPCs) for SCs [46]. They found that $900 \text{ }^\circ\text{C}$ -derived NPC was optimal to deliver the maximum capacitance. First, higher temperatures assisted the carbonization that increased the conductivity. Additionally, extra high temperatures ($1000 \text{ }^\circ\text{C}$) caused the loss of heteroatom such as N, thus, decreasing the PC and, therefore total capacitance. In addition, creating a mesoporous shell or hollow structure in ZIF-8 can largely benefit the capacitance enhancement after pyrolysis. This is also demonstrated by Zhang et al.'s work by using macroporous ZIF-8 [47], since the hierarchically porous carbons can adsorb more ions. The synthesis strategy of NPC from MOFs is far more than simple carbonization. To diversify the NPC with various structures or compositions, some precursor-control protocols, such as heteroatom doping, shape/orientation control, and hybridization with other functional materials were reported (Figure 5a) [48].

Nevertheless, during this process, the intrinsic pore channels of MOFs are inevitably destroyed, leaving the carbonized structures with decreased surface area [49–51]. To address this issue, Khan and coworkers [52] added activated carbon (AC) into the skeleton of MOF-5 for cocarbonization. The results indicated an increased specific surface area

and pore volume: $677 \text{ m}^2/\text{g}$ and $0.412 \text{ cm}^3/\text{g}$, respectively. As expected, it delivered a larger specific capacitance of 300 F g^{-1} at 1.5 A g^{-1} and retained 91.5% of this capacity after 3000 cycles. Likewise, Li et al. [53] synthesized single crystal-ordered macroporous MOF (SIM-HKUST-1) using polystyrene as a hard template, followed by pyrolysis into macroporous carbon (IM-HPC) (Figure 5b). The hierarchically porous structure (Figure 5c) displayed excellent cyclic stability when used as an SC electrode (Figure 5d). To further enhance the electrochemical performance, researchers doped heteroatoms in the carbon skeleton. For example, Huang et al. [54] employed ZnO nanorods as templates to produce ZIF-8@ZnO hybrid. When the hybrid was subjected to high-temperature carbonization under KOH activation, it achieved N-doped porous carbon nanosheet (Figure 5e) with a large specific surface area of $1190 \text{ m}^2/\text{g}$ and a specific capacitance of 290 F g^{-1} at a current density of 1 A g^{-1} . In addition, after 10,000 consecutive cycles, it retained 94% of its original capacity (Figure 5f). In fact, many MOF ligands naturally possess N atoms that satisfy in situ doping during pyrolysis. For instance, Gu et al. [55] prepared NPMOF with ligands containing pentabasic N atoms (Figure 5g). In contrast with imidazole-based ZIFs, more N contents doping resulted in an enhanced specific capacitance up to 220 F g^{-1} , highlighting the pseudocapacitive effect of heteroatoms.

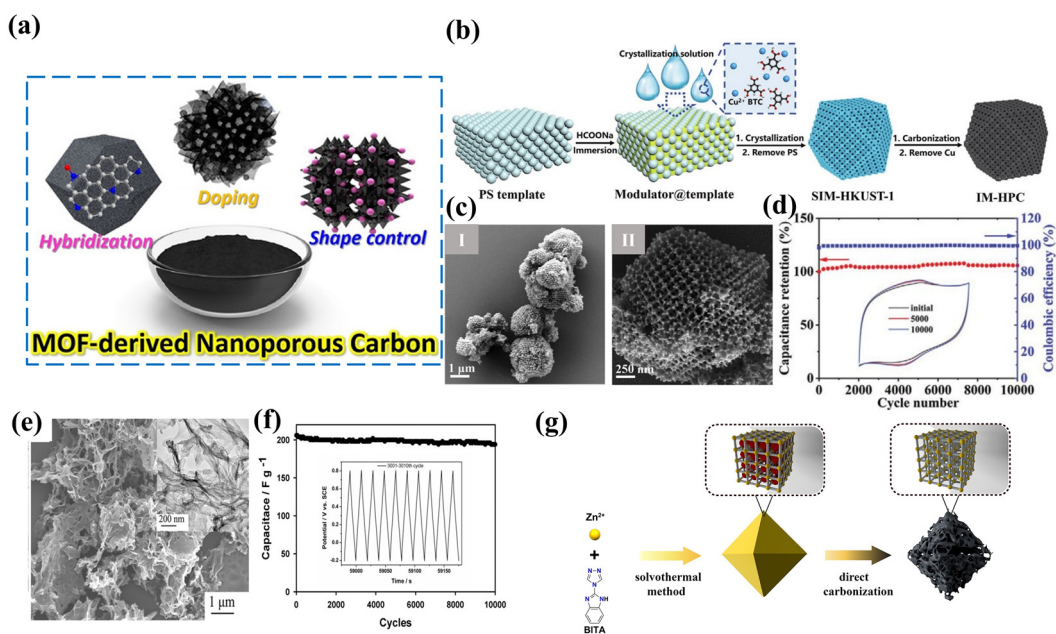


Figure 5. (a) Strategies to enhance the properties and performance of MOF-derived carbons. Reproduced with permission from ref. [48]. Copyright 2019 Wiley-VCH Verlag GmbH & Co. KGaA, Weinheim. (b) Schematic illustration of preparation of SIM-HKUST-1 and its derivative carbon material. (c) SEM images of carbon materials derived from SIM-HKUST-1 at different magnifications. (d) Long-term cycle performance and Coulombic efficiency of IM-HPC at a scan rate of 50 mV s^{-1} . Inset: initial CV curve and CV curves after 5000 and 10,000 cycles. Reproduced with permission from ref. [53]. Copyright 2020 WILEY-VCH. (e) TEM images of N-PCTs-1000. (f) The charge–discharge stability of NPCS at a current density of 20 A g^{-1} in $1 \text{ M H}_2\text{SO}_4$ aqueous solution. Reproduced with permission from ref. [54]. Copyright 2018 Elsevier. (g) MOF-derived porous carbons and single crystal structure of NPMOF. Reproduced with permission from ref. [55]. Copyright 2020 Elsevier.

4.2. Transition Metal Oxide

Metal (Co, Ni, Mn, and Zn et al.) oxides derived from MOFs have been widely studied for SCs, since they usually deliver ultra-high PCs. For instance, Meng et al. [56] obtained porous Co_3O_4 particles through a two-step calcination of Co-MOF, which exhibited a high specific capacitance of 150 F g^{-1} at a current density of 1 A g^{-1} (Figure 6a). Similarly, Zheng et al. [57] fabricated $\text{Co}_3\text{O}_4/\text{Co-MOF}$ heterojunction in a highly alkaline

environment, where Co ions in MOFs tended to partially form Co oxides (Figure 6a). The Co_3O_4 @Co-MOF with a leaf-like nanosheet morphology thus exhibited excellent stability under alkaline electrolytes (Figure 6b). Moreover, Co_3O_4 nanoparticles on the surface of Co-MOF significantly expanded the redox active sites, leaving capacitance of 1020 F g^{-1} at 0.5 A g^{-1} (Figure 6c), and great cycle stability over 5000 cycles, with a capacitance retention rate of almost 96.7% at 5 A g^{-1} (Figure 6d). Furthermore, Wu et al. [58] created nickel cobalt (Ni-Co) oxide nanocages from binary MOFs, which presented greater electrochemical performance than single cobalt oxide-based electrodes. Babu et al. [59] also synthesized a bimetal MOF-derived nickel–manganese oxide for supercapacitor electrodes by solvothermal reaction and subsequent calcination. The resulting NiMn_2O_4 exhibited a spinel structure (Figure 6e) with a high specific capacitance of 1387 F g^{-1} (Figure 6f) and significant cycle life at a current density of 1 A g^{-1} (80% capacity retention after 6500 cycles). However, metal-oxide particles are easy to aggregate and deform during charging and discharging. To solve this problem, some substrates were utilized to grow MOF precursors in situ. For instance, Lim et al. [60] directly synthesized 2D bimetallic cobalt-based MOF on a carbon substrate and converted it into porous leaf-like metal oxides ((Figure 6g,h). It suggested that bimetal ZnCo_2O_4 prepared from Co/Zn-MOF conveyed maximum conductivity, electrochemical properties and specific capacity than other cases. Also, outstanding mechanical stability and flexibility were guaranteed. Additionally, the growing MOFs in situ on flexible substrates can be used as freestanding electrodes. For instance, Acharya et al. [61] uniformly grew bimetal and monometal MOF arrays on carbon fibers and converted them into Ni-Fe-O/NPC@PCNFs-400 and Fe_2O_3 /NPC@PCNFs (Figure 6i,j). They then assembled them into asymmetrical SCs where 88.5% of its original exceptional specific capacitance (1419 F g^{-1} at 1 A g^{-1}) can be maintained (Figure 6k).

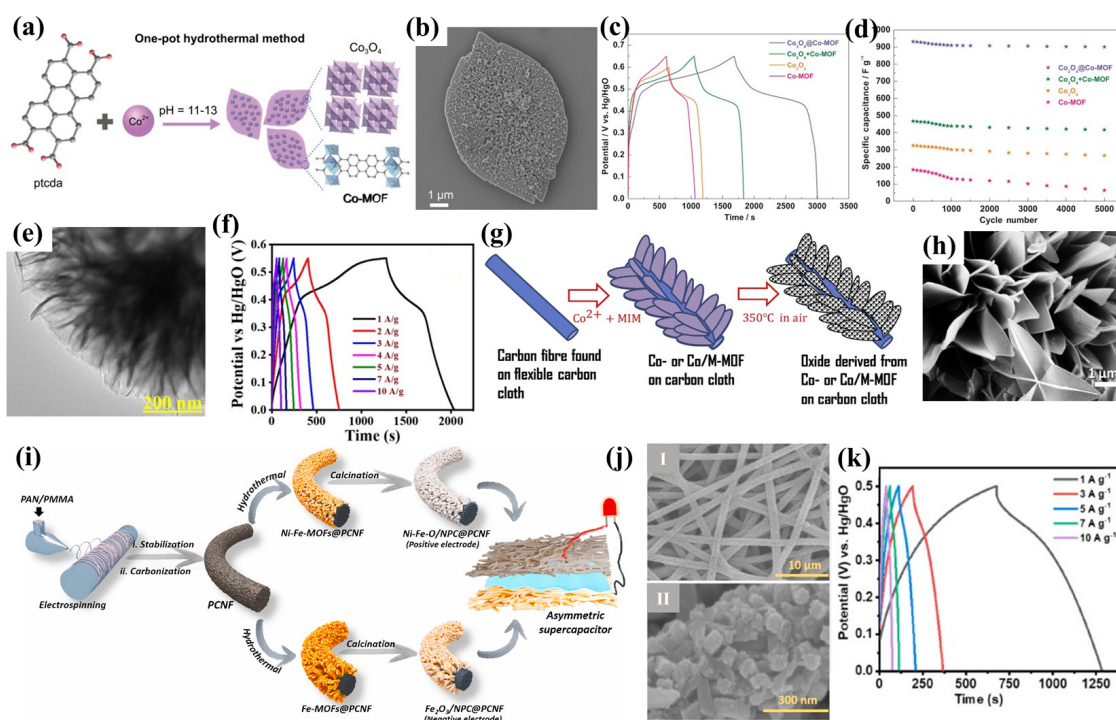


Figure 6. (a) Schematic illustration of one-pot hydrothermal synthesis of Co_3O_4 @Co-MOF composite. (b) SEM images of Co_3O_4 @Co-MOF. (c) GCD curves at a current density of 0.5 A g^{-1} (d) Cycling performance at 5 A g^{-1} for 5000 cycles. Reproduced with permission from ref. [57]. Copyright 2020 National Science Review. (e) TEM image of NiMn_2O_4 . (f) Chronopotentiometry at various current densities Reproduced with permission from ref. [59]. Copyright 2022 Elsevier. (g) Schematic illustration of fabrication process, where 2D nanosheets of metallic oxides derived from MOFs are

obtained from the metallic MOF precursor. (h) SEM images of oxide derived from Co/Zn-MOF. Reproduced with permission from ref. [60]. Copyright 2018 Elsevier. (i) Schematic representation of fabrication of electrode materials synthesis for ASC device. (j) FE-SEM image of Ni-Fe-MOFs@PCNFs. (k) GCD graphs at various current densities. Reproduced with permission from ref. [61]. Copyright 2022 Elsevier.

4.3. Metal Hydroxides

Similar to metal oxide, metal hydroxides, especially layered double hydroxides (LDH) with a spinal layered structure generated from MOFs, are also ideal electrodes for SCs due to the large theoretical PCs [62,63]. For example, Cao et al. [64] used Co-Ni-MOF as a sacrificial template to prepare Ni-Co LDH through alkaline hydrolysis. After electrochemical tests, the Ni-Co LDH showed good cycle stability, low resistance, and a specific capacity of 1265 F g^{-1} at a current density of 1 A g^{-1} . Huang et al. [65] also synthesized Co/Ni LDH under mild conditions ($50 \text{ }^\circ\text{C}$) through a simple solvothermal method. The as-obtained Co/Ni-LDH presented a unique 2D nanosheet array alignment with a high specific capacity and a 92.3% capacitive retention after 10,000 cycles. Also, hollow Ni-Co LDH can be synthesized through ZnO templated Co/Ni MOF etching. In Liu et al.'s work [66], they first prepared a ZnO nanorod array in carbon fiber cloth (CFC). Afterwards, a Ni-Co MOFs shell was grown on a ZnO nanorod core. Then, Ni-Co MOFs were etched to be LDH, followed by removing the ZnO template. Finally, hollow LDH/CFC superstructures were successfully obtained (Figure 7a). It is interesting that fungus-like Ni-Co@Ni-Co-LDH grew uniformly along the axis of CFC (Figure 7b,c). The LDH structure also exhibited a huge top and a small bottom (Figure 7d), where the top was composed of LDH (Figure 7e). Thus, the architecture increased the surface area and showed ultrahigh capacitance of 2200 F g^{-1} at 5 A g^{-1} .

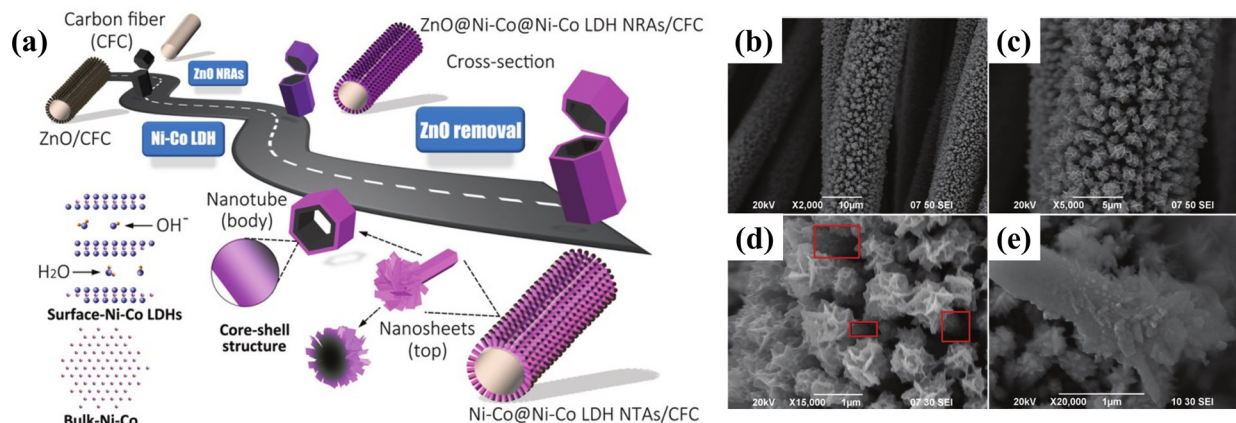


Figure 7. (a) Schematic diagram of the preparation procedures of the hierarchically porous Ni-Co@Ni-Co LDH NTAs on CFC. (b–e) SEM images of Ni-Co@Ni-Co LDH NRAs on ZnO template. Reproduced with permission from ref. [66]. Copyright 2017 WILEY-VCH.

Moreover, there are metal sulfides [67,68], metal phosphides [69], and metal selenides [70] derived from MOFs as well for SCs. However, their power density and cycle stability remain to be improved.

5. MOF Composite Materials

In order to directly enhance the electrochemical performance, MOFs can be mixed with highly conductive materials as SC electrodes [71,72]. Generally, conductive nonmetallic materials include carbon materials, and conductive polymers, etc. While metallic materials involve metal oxides, metal hydroxides, and pure metals, etc. The exploitation of MOF composites for SCs further enriches the species of MOFs in the energy storage field.

5.1. MOFs and NonMetallic Materials

Currently, nonmetallic materials used in MOF composites are generally graphene oxide, carbon fibers, carbon nanotubes, polyaniline, polypyrrole, etc. There are three basic fabrication strategies for MOF composites: (1) direct mixing by H-bonding, conjugation or ionic interaction, (2) in situ growing MOFs on nonmetallic materials and (3) epitaxial growing MOF-derived metal oxides on MOFs to form the heterojunction.

For instance, Hosseinian et al. [73] fabricated a rGO/ZIF-67 composite by growing ZIF-67 nanocrystals on rGO. At a current density of 1 A g^{-1} , the specific capacitance of rGO/ZIF-67 was 210 F g^{-1} , which is more than double that of ZIF-67 (103.6 F g^{-1}). Ramachandran et al. [74] adopted a wet technique to create the cerium (Ce) metal organic matrix composites Ce-MOF/GO and Ce-MOF/CNT (Figure 8a,b). Compared with Ce-MOF/CNT, Ce-MOF/GO revealed larger specific capacitance with 2221.2 F g^{-1} at a current density of 1 A g^{-1} . More contact with Ce-MOF is attributed to the layered structure of GO. Additionally, the oxygen-containing groups in GO can promote ion migration at the electrode/electrolyte interface. Furthermore, Xu et al. [75] directly grew rolled a CoNi-MOF nanosheet array on carbon cloth (CC) (Figure 8c,d), which exhibited good conductance and outstanding cycle stability (Figure 8e). Likewise, Ibrahim et al. [76] introduced Ni-MOF on graphene through a simple mixing method. Compared with growing MOF crystals in situ in graphene, the Ni-MOF was scattered and intensively attached on both sides of GO layer (Figure 8f), therefore delivering a high specific capacitance of 70.41 F g^{-1} at 1 A g^{-1} . Different from mixing, sometimes the in situ hydrothermal method can generate MOF polyhedra crystal composites (Ni-BTC@GO) (Figure 8g,h) [77]. The maximum capacitance of Ni-BTC@GO reached up to 1199 F g^{-1} at 1 A g^{-1} , larger than the mixing case. Conductive polymers (CPS) are common components for MOF composites as well. Among CPS, polyaniline (PANI) is the most widely reported for SCs. For example, Shao et al. [78] polymerized PANI on the lattice of UIO-66 with an interpenetrating network through interactions to enhance carrier conduction (Figure 8i). To make the electrode flexible, Xu et al. [79] prepared ZIF-L/PANI on CFC by alternative soaking (Figure 8j). The as-fabricated electrodes can be used for wearable devices. Moreover, Sara et al. [80] deposited ZIF-67 on the PANI nanotube, wrapped by graphene (Figure 8l). The composites exhibited increased conductivity and greater capacitive capacity than a single ZIF-67 crystal.

5.2. MOFs and Metallic Materials

The redox centers of MOFs can be extended when combining MOFs with metal species (such as pure metals, metal oxide nanoparticles, metal sulfides, etc.). For example, Hussain et al. [81] fabricated a flexible electrode by solvothermal treatment of Zn-Co-MOF@CuO on CuO skeleton (Figure 9a). The prepared electrode showed excellent flexibility even after being subjected to various bending. The introduction of CuO gifted the MOF composite metallic properties. At 1 A g^{-1} , the energy density of the supercapacitor can reach 41 Wh kg^{-1} . Even after 20,000 constant charge and discharge cycles, the supercapacitor still maintained 97% of its initial capacity (Figure 9b). Likewise, Wang et al. [82] constructed a new vertically arranged Co-MOF@CoNiO₂ core shell composite material by chemical vapor depositing Co-MOF shell layers on the CoNiO₂ core (Figure 9c). The as-synthesized Co-MOF@CoNiO₂ electrode displayed a specific capacitance of $\sim 571 \text{ F g}^{-1}$. Similarly, Shi et al. [83] built a vertically oriented Ni-MOF@Co(OH)₂ array by using Ni foam as both substrate and precursor (Figure 9d). The MOF/metal composites delivered ultra-high capacitance of 1448 F g^{-1} at 2 A g^{-1} . In addition, Lu et al. [84] synthesized an order of Ni-HHTP@Ni(OH)₂ nanoarrays by employing Ni(OH)₂ nanosheets as a template (Figure 9e). As a positive electrode for asymmetric SCs, the stability of Ni-HHTP@Ni(OH)₂ was improved with 98% retention rate after 5000 cycles even at 3 A g^{-1} , superior to pristine Ni(OH)₂.

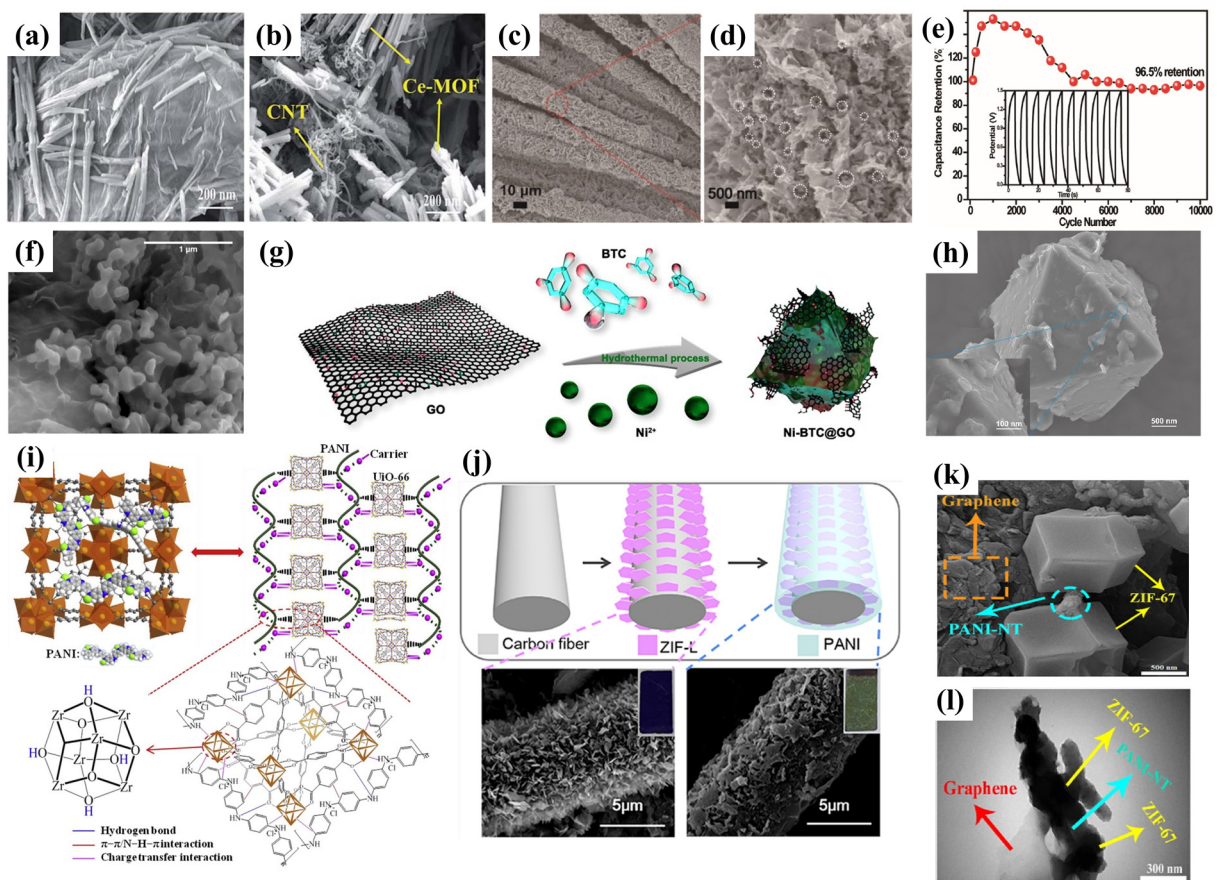


Figure 8. (a) SEM images of Ce-MOF/GO composite. (b) SEM image of Ce-MOF/CNT composite. Reproduced with permission from ref. [74]. Copyright 2018 The Royal Society of Chemistry. (c,d) SEM images of CC/CoNi-MOF. (e) Cycle stability at 20 mA cm⁻². Inset is the last 10 cycles. Reproduced with permission from ref. [75]. Copyright 2020 Elsevier. (f) FESEM morphology of Ni-MOF/GO. Reproduced with permission from ref. [76]. Copyright 2021 Elsevier. (g) Preparation process of the Ni-BTC@GO composites. (h) SEM image of Ni-BTC@GO. Reproduced with permission from ref. [77]. Copyright 2023 American Chemical Society. (i) Schematic illustration of interaction and carrier conduction between PANI and UiO-66. Reproduced with permission from ref. [78]. Copyright 2018 Elsevier. (j) Schematic diagram of CFP/ZIF-L/PANI formation. Reproduced with permission from ref. [79]. Copyright 2021 American Chemical Society. (k) FESEM images of Graphene@ZIF-67/PANI-NT composite. (l) TEM image of Graphene@ZIF-67/PANI-NT composite. Reproduced with permission from ref. [80]. Copyright 2022 Elsevier.

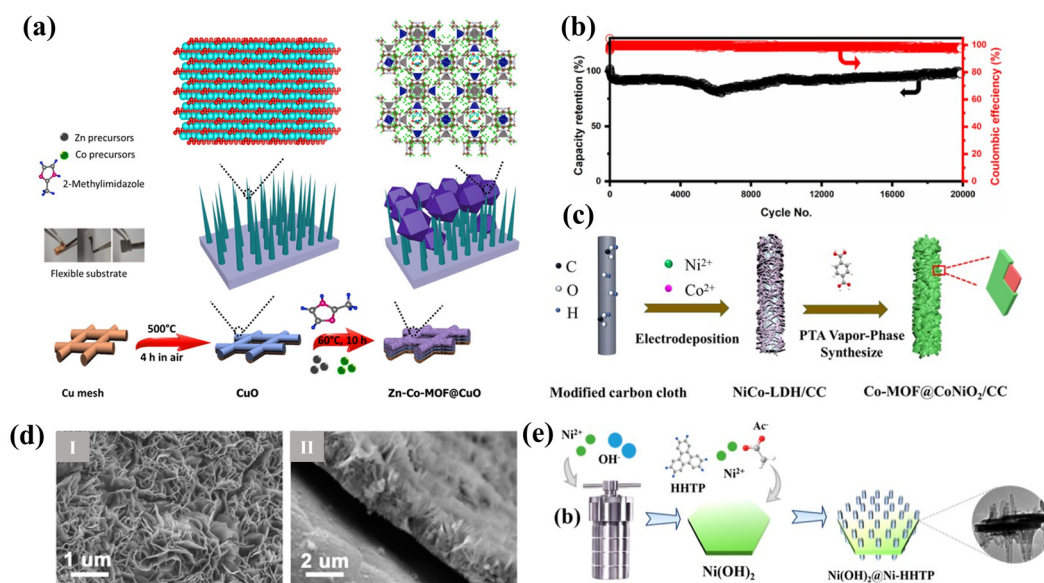


Figure 9. (a) Schematic design of the development of CuO and Zn-Co-MOF@CuO. (b) Stability of Zn-Co-MOF@CuO during 10,000 cycles. Reproduced with permission from ref. [81]. Copyright 2022 Elsevier. (c) Schematic illustration of the fabrication of Co-MOF@CoNiO₂ core/shell nanosheet arrays on the carbon cloth substrate. Reproduced with permission from ref. [82]. Copyright 2020 American Chemical Society. (d) SEM characterization (top view) and cross-section SEM image of Ni-MOF@Co(OH)₂. Reproduced with permission from ref. [83]. Copyright 2021 Elsevier. (e) Schematic diagram of the fabrication of Ni(OH)₂@Ni-HHTP nanoarrays. Reproduced with permission from ref. [84]. Copyright 2022 American Chemical Society.

6. Conclusions and Perspectives

The research advancements of MOF-based materials in the field of SCs are comprehensively discussed in this review. It can be concluded that pure MOFs and their derivative materials exhibit great potential in SCs. To enhance the electrochemical efficiency and structural stability of MOFs, researchers have devoted effort to MOF hybrids or creating MOF derivatives. For example, by using MOF as a template or serving as the precursor to prepare metal–carbon materials, it not only retains the intrinsic feature of MOFs, such as a polyhedron shape for nanoreactors and high metal loading, but also improves its structural stability and electrochemical performance. In addition, MOFs can be hybridized with other conductive materials (carbon materials, conductive polymers, metal materials, etc.), thus, further enhancing electron transfer and expanding active sites. Here, we also listed some issues required to be addressed at this stage and in future research:

- (1) Materials preparation of MOF. Currently, the majority of MOFs are produced in laboratories using techniques like hydrothermal, solvothermal synthesis, etc. However, these techniques may have some limitations including low yield, high energy consumption and time consuming. It prevents them from large-scale industrial production and practical applications. Moreover, some organic compounds and solvents for MOF preparation are toxic while the postprocessing is sometimes expensive. Therefore, to develop a green and effective organic ligand with recycling technology to reduce costs is significant.
- (2) High conductance and high capacitance. Most pure MOFs have large resistance and poor conductivity, which is disadvantageous for SCs, although some newly reported conductive MOFs such as Ni₃(HITP)₂ showcase potential practicability. However, the performance also relies on the electrodes, e.g., ionic liquid rather than being highly stable in aqueous acid or alkaline. The conjugated system can facilitate fast electron transport, yet the energy storage behavior is sometimes complicated and independent

of pore sizes. Hence, to explore new types of MOFs with both excellent properties is still challenging.

- (3) The design of MOF-based SC devices. The device design can maximize the electrochemical performance of SCs and broaden the application scenarios. For example, similar to graphene-based devices, flexible microcapacitors with 2D MOFs grown in situ on the intercalation electrode can simultaneously satisfy powering unit and wearable requirements. In the future, there will be more integrated units based on MOFs. For instance, the pore nature of MOFs can be expanded to fabricate MOF gas sensors but being self-powered by MOF-based SCs.
- (4) Mechanism. Currently, the accurate mechanisms of electrochemical storage of MOFs are still ambiguous. The capacitive capacity and whether it belongs to faradaic pseudocapacitive or EDLC are depending on the electrolytes. Moreover, for binary and multimetallic MOFs, the mechanism of how different components influence electrochemical performance has not yet been figured out. Therefore, there is a long way to go to fully explore it.
- (5) Advanced characterizations. Cs-corrected TEM and in situ spectrum now can ascertain the specific atomic structural changes of metal oxide electrodes, especially in the research of catalysts and batteries. For MOFs applied in SCs, due to the stability and organic/inorganic features, the advanced characterizations are still lacking. Moreover, for highly crystalline MOFs, during charging and discharging, there may be lattice strain to induce capacitance attenuation. Nevertheless, it has seldom been reported, due to the limitations of advanced characterizations.

Finally, the advantages and disadvantages of MOFs for SCs discussed above may provide a broad understanding of the structure–function relationship of these materials in the energy storage field. For pure MOFs, first, the optimization of the framework dimensionality, ligand functionalization, metal constitution and pore size can assist in the improvement of the capacitance [85,86]. In addition, the rising trend of conductive MOFs can further boost the opportunities of extending pure MOFs for SCs [87]. However, the stability of pure MOFs for SCs is still challenging; additionally, the behind degradation mechanisms have seldom been explored. For MOF-derived carbon materials, although they feature advantages of high conductance and stable EDLCs, the optimal pyrolysis conditions such as carbonization temperatures, gases atmosphere are difficult to make a uniform standard [88,89]. Moreover, the carbonization process requiring high-temperature heating is also energy-consuming. For MOF-based composites, the second or third component is indeed helpful to not only expand the capacitance but also enhance stability. Nevertheless, in most cases, MOFs have a weakening influence on the structure activity, against the deep understanding of charge–discharge mechanisms from the perspective of MOFs [90]. Additionally, different from porous carbons with amorphous structures that are difficult to model, computational studies such as molecular dynamic simulation make it easy to predict the charge–discharge behavior of MOFs with crystalline structures. It can provide guidelines for pure MOFs design for SCs in the future. We also envision that there would be more miniaturized energy devices by directly growing MOF layers for flexible and wearable electronics.

Author Contributions: Conceptualization, X.W. and J.W.; Investigation, Y.Z. and P.S.; Resources, X.W.; Writing original draft preparation, Y.Z.; Writing review and editing, Y.Z. and J.W.; Visualization, X.W.; Supervision, X.W. All authors have read and agreed to the published version of the manuscript.

Funding: This project was funded by National Science Foundation of China (NSFC), grant number 52103178, 00605054A1002; Sixth Two-hundred Talent B plan of Sichuan University and the Science and Technology Project of Sichuan Province, grant number 2023NSFSC0997.

Data Availability Statement: Data that support the findings of this study is contained within the article.

Acknowledgments: The authors acknowledge the National Science Foundation of China (NSFC) (Grant 52103178, 00605054A1002), Sixth Two-hundred Talent B plan of Sichuan University and the Science and Technology Project of Sichuan Province (Grant 2023NSFC0997).

Conflicts of Interest: The authors declare no conflict of interest.

Appendix A

Table A1. The comparison of MOF-based electrode materials for SCs.

Samples	Metal Sites	Electrolyte	Maximum Capacitance (F g ⁻¹)	Measured Current Density (A g ⁻¹)	Cycle Life	Ref
Co-LMOF	Co	1 M KOH	2474	1	94.3% after 2000 cycles	[30]
Co-MOF	Co	5 M KOH	2564	1	95.8% after 3000 cycles	[31]
Co-MOFs	Co	3 M KOH	958.1	2	92.3% after 3000 cycles	[32]
Co-BTC	Co	1M NaOH	657	0.5	81.4% after 3000 cycles	[33]
Co-MOF-74	Co	3 M KOH	164.2	0.5	75% after 1500 cycles	[34]
Ni-MOF	Ni	3 M KOH	988	1.4	96.5% after 5000 cycles	[36]
Ni-MOF	Ni	3 M KOH	1057	1	70% after 2500 cycles	[37]
Ni/Co-MOF	Ni/Co	2 M KOH	758	1	75% after 5000 cycles	[39]
Ni/Co-MOF	Ni/Co	2 M KOH	2860	1	90% after 2000 cycles	[40]
MOF-5	Zn	6 M KOH	300	1.5	91% after 3000 cycles	[52]
ZIF-8@ZnO	Zn	1M H ₂ SO ₄	290	1	94% after 10,000 cycles	[54]
NPMOF	Zn	6 M KOH	220	1	99.1% after 10,000 cycles	[55]
Co ₃ O ₄ @Co-MOF	Co	3 M KOH	1020	0.5	96.7% after 5000 cycles	[57]
Ni/Mn-MOF	Ni/Mn	1 M KOH	1387	1	80% after 6500 cycles	[59]
PCNFs	Ni	3 M KOH	1419	1	88.5% after 10,000 cycles	[61]
Ni-Co LDH	Ni/Co	1 M NaOH	2200	5	98.6% after 3000 cycles	[66]
Ce-MOF/GO	Ce	3 M KOH	2221.2	1	87% after 5000 cycles	[74]
CC/CoNi-MOF	Ni/Co	1 M KOH	846	1	96.5% after 10,000 cycles	[75]
Ni-BTC@GO	Ni	3 M KOH	1199	1	84.5% after 5000 cycles	[77]
Co-MOF@CoNiO ₂	Co	6 M KOH	757.2	1	80.6% after 5000 cycles	[82]
Ni-MOF@Co(OH) ₂	Ni	1 M KOH	1448	2	87.3% after 8000 cycles	[83]

References

- Sanyal, S.; Wuebbles, D.J. The Potential Impact of a Clean Energy Society on Air Quality. *Earths Future* **2022**, *10*, e2021EF002558. [CrossRef]
- Xu, J.K.; Lei, J.F.; Ming, N.N.; Zhang, C.T.; Huo, K.F. Rational Design of Wood-Structured Thick Electrode for Electrochemical Energy Storage. *Adv. Funct. Mater.* **2022**, *32*, 2204426. [CrossRef]
- Roy, B.K.; Tahmid, I.; Rashid, T.U. Chitosan-based materials for supercapacitor applications: A review. *J. Mater. Chem. A* **2021**, *9*, 17592–17642. [CrossRef]
- Liu, Y.; Qian, J.L.; Shi, Y.X.; Xu, Y.; Mao, Y.J.; Lv, R.G.; Huang, B.; Sun, Y.Z.; Zhao, Z.Y.; Chang, Y.N.; et al. Latest advances of metal-organic frameworks-based materials for supercapacitors. *Sustain. Mater. Technol.* **2023**, *36*, e00588. [CrossRef]
- Fagiolari, L.; Sampo, M.; Lamberti, A.; Amici, J.; Francia, C.; Bodoardo, S.; Bella, F. Integrated energy conversion and storage devices: Interfacing solar cells, batteries and supercapacitors. *Energy Storage Mater.* **2022**, *51*, 400–434. [CrossRef]
- Shah, S.S.A.; Najam, T.B.; Bashir, M.S.; Peng, L.S.; Nazir, M.A.; Javed, M.S. Single-atom catalysts for next-generation rechargeable batteries and fuel cells. *Energy Storage Mater.* **2022**, *45*, 301–322. [CrossRef]
- Yang, Y.; Hoang, M.T.; Bhardwaj, A.; Wilhelm, M.; Mathur, S.; Wang, H.X. Perovskite solar cells based self-charging power packs: Fundamentals, applications and challenges. *Nano Energy* **2022**, *94*, 106910. [CrossRef]
- Li, X.; Wang, J. One-dimensional and two-dimensional synergized nanostructures for high-performing energy storage and conversion. *Infomat* **2020**, *2*, 3–32. [CrossRef]
- Ega, S.P.; Srinivasan, P. Quinone materials for supercapacitor: Current status, approaches, and future directions. *J. Energy Storage* **2022**, *47*, 103700. [CrossRef]
- Zhang, D.; Tan, C.; Zhang, W.Z.; Pan, W.J.; Wang, Q.; Li, L. Expanded Graphite-Based Materials for Supercapacitors: A Review. *Molecules* **2022**, *27*, 716. [CrossRef]
- Zhong, M.Z.; Zhang, M.; Li, X.F. Carbon nanomaterials and their composites for supercapacitors. *Carbon Energy* **2022**, *4*, 950–985. [CrossRef]

12. Tang, Y.Q.; Shen, H.M.; Cheng, J.Q.; Liang, Z.B.; Qu, C.; Tabassum, H.; Zou, R.Q. Fabrication of Oxygen-Vacancy Abundant NiMn-Layered Double Hydroxides for Ultrahigh Capacity Supercapacitors. *Adv. Funct. Mater.* **2020**, *30*, 1908223. [[CrossRef](#)]
13. Naseri, F.; Karimi, S.; Farjah, E.; Schaltz, E. Supercapacitor management system: A comprehensive review of modeling, estimation, balancing, and protection techniques. *Renew. Sust. Energ. Rev.* **2022**, *155*, 111913. [[CrossRef](#)]
14. Zhao, Y.H.; He, X.Y.; Chen, R.R.; Liu, Q.; Liu, J.Y.; Yu, J.; Li, J.Q.; Zhang, H.S.; Dong, H.X.; Zhang, M.L.; et al. A flexible all-solid-state asymmetric supercapacitors based on hierarchical carbon cloth@CoMoO₄NiCo layered double hydroxide core-shell heterostructures. *Chem. Eng. J.* **2018**, *352*, 29–38. [[CrossRef](#)]
15. Sheberla, D.; Bachman, J.C.; Elias, J.S.; Sun, C.J.; Shao-Horn, Y.; Dinca, M. Conductive MOF electrodes for stable supercapacitors with high areal capacitance. *Nat. Mater.* **2017**, *16*, 220–224. [[CrossRef](#)]
16. Zhou, H.C.; Kitagawa, S. Metal-Organic Frameworks (MOFs). *Chem. Soc. Rev.* **2014**, *43*, 5415–5418. [[CrossRef](#)]
17. Liu, M.J.; Xing, Z.P.; Li, Z.Z.; Zhou, W. Recent advances in core-shell metal organic frame-based photocatalysts for solar energy conversion. *Coord. Chem. Rev.* **2021**, *446*, 214123. [[CrossRef](#)]
18. Xu, B.; Zhang, H.B.; Mei, H.; Sun, D.F. Recent progress in metal-organic framework-based supercapacitor electrode materials. *Coord. Chem. Rev.* **2020**, *420*, 213438. [[CrossRef](#)]
19. Xu, J.; Peng, Y.; Xing, W.Q.; Ding, Z.Y.; Zhang, S.T.; Pang, H. Metal-organic frameworks marry carbon: Booster for electrochemical energy storage. *J. Energy Storage* **2022**, *53*, 105104. [[CrossRef](#)]
20. Zheng, S.Q.; Lim, S.S.; Foo, C.Y.; Haw, C.Y.; Chiu, W.S.; Chia, C.H.; Khiew, P.S. Recent Progress on the Applications of Carbonaceous and Metal-Organic Framework Nanomaterials for Supercapacitors. *Front. Mater.* **2021**, *8*, 777149. [[CrossRef](#)]
21. Li, Q.; Xu, Y.X.; Zheng, S.S.; Guo, X.T.; Xue, H.G.; Pang, H. Recent Progress in Some Amorphous Materials for Supercapacitors. *Small* **2018**, *14*, 1800426. [[CrossRef](#)] [[PubMed](#)]
22. Ajdari, F.B.; Kowsari, E.; Shahrak, M.N.; Ehsani, A.; Kiaei, Z.; Torkzaban, H.; Ershadi, M.; Eshkalak, S.K.; Haddadi-Asl, V.; Chinnappan, A.; et al. A review on the field patents and recent developments over the application of metal organic frameworks (MOFs) in supercapacitors. *Coord. Chem. Rev.* **2020**, *422*, 213441. [[CrossRef](#)]
23. Fleischmann, S.; Mitchell, J.B.; Wang, R.C.; Zhan, C.; Jiang, D.E.; Presser, V.; Augustyn, V. Pseudocapacitance: From Fundamental Understanding to High Power Energy Storage Materials. *Chem. Rev.* **2020**, *120*, 6738–6782. [[CrossRef](#)] [[PubMed](#)]
24. Tang, Y.Q.; Liang, Z.B.; Jin, Y.K.; Gao, S.; Zou, R.Q. Understanding and tackling lattice manganese exfoliation and deactivation of battery-type NiMn-LDH in fast electrochemical energy storage. *J. Mater. Chem. A* **2021**, *9*, 23286–23295. [[CrossRef](#)]
25. Sun, Y.Z.; Liu, Y.; Han, Y.T.; Li, Z.Y.; Ning, G.Q.; Xing, R.; Ma, X.L. Effects of thermal transformation on graphene-like lamellar porous carbon and surface-contributed capacitance. *Mater. Today Commun.* **2021**, *29*, 102982. [[CrossRef](#)]
26. Xu, B.Y.; Zheng, M.B.; Tang, H.; Chen, Z.X.; Chi, Y.; Wang, L.; Zhang, L.; Chen, Y.Y.; Pang, H. Iron oxide-based nanomaterials for supercapacitors. *Nanotechnology* **2019**, *30*, 204002. [[CrossRef](#)]
27. Liu, Y.; Zhang, B.H.; Yang, Y.Q.; Chang, Z.; Wen, Z.B.; Wu, Y.P. Polypyrrole-coated alpha-MoO₃ nanobelts with good electrochemical performance as anode materials for aqueous supercapacitors. *J. Mater. Chem. A* **2013**, *1*, 13582–13587. [[CrossRef](#)]
28. Zhao, Y.H.; He, X.Y.; Chen, R.R.; Liu, Q.; Liu, J.Y.; Song, D.L.; Zhang, H.S.; Dong, H.X.; Li, R.M.; Zhang, M.L.; et al. Hierarchical NiCo₂S₄@CoMoO₄ core-shell heterostructures nanowire arrays as advanced electrodes for flexible all-solid-state asymmetric supercapacitors. *Appl. Surf. Sci.* **2018**, *453*, 73–82. [[CrossRef](#)]
29. Díaz, R.; Orcajo, M.G.; Botas, J.A.; Calleja, G.; Palma, J. Co8-MOF-5 as electrode for supercapacitors. *Mater. Lett.* **2012**, *68*, 126–128. [[CrossRef](#)]
30. Liu, X.; Shi, C.; Zhai, C.; Cheng, M.; Liu, Q.; Wang, G. Cobalt-Based Layered Metal-Organic Framework as an Ultrahigh Capacity Supercapacitor Electrode Material. *ACS Appl. Mater. Interfaces* **2016**, *8*, 4585–4591. [[CrossRef](#)]
31. Yang, J.; Ma, Z.; Gao, W.; Wei, M. Layered Structural Co-Based MOF with Conductive Network Frames as a New Supercapacitor Electrode. *Chemistry* **2017**, *23*, 631–636. [[CrossRef](#)] [[PubMed](#)]
32. Ramachandran, R.; Zhao, C.; Luo, D.; Wang, K.; Wang, F. Morphology-dependent electrochemical properties of cobalt-based metal organic frameworks for supercapacitor electrode materials. *Electrochim. Acta* **2018**, *267*, 170–180. [[CrossRef](#)]
33. Zhang, H.; Wang, J.; Sun, Y.; Zhang, X.; Yang, H.; Lin, B. Wire spherical-shaped Co-MOF electrode materials for high-performance all-solid-state flexible asymmetric supercapacitor device. *J. Alloys Compd.* **2021**, *879*, 160423. [[CrossRef](#)]
34. Wang, C.; Li, X.; Yang, W.; Xu, Y.; Pang, H. Solvent regulation strategy of Co-MOF-74 microflower for supercapacitors. *Chin. Chem. Lett.* **2021**, *32*, 2909–2913. [[CrossRef](#)]
35. Jiao, Y.; Pei, J.; Yan, C.S.; Chen, D.H.; Hu, Y.Y.; Chen, G. Layered nickel metal-organic framework for high performance alkaline battery-supercapacitor hybrid devices. *J. Mater. Chem. A* **2016**, *4*, 13344–13351. [[CrossRef](#)]
36. Yan, Y.; Gu, P.; Zheng, S.; Zheng, M.; Pang, H.; Xue, H. Facile synthesis of an accordion-like Ni-MOF superstructure for high-performance flexible supercapacitors. *J. Mater. Chem. A* **2016**, *4*, 19078–19085. [[CrossRef](#)]
37. Du, P.; Dong, Y.; Liu, C.; Wei, W.; Liu, D.; Liu, P. Fabrication of hierarchical porous nickel based metal-organic framework (Ni-MOF) constructed with nanosheets as novel pseudo-capacitive material for asymmetric supercapacitor. *J. Colloid Interface Sci.* **2018**, *518*, 57–68. [[CrossRef](#)]
38. Shen, W.; Guo, X.; Pang, H. Effect of Solvothermal Temperature on Morphology and Supercapacitor Performance of Ni-MOF. *Molecules* **2022**, *27*, 8226. [[CrossRef](#)]

39. Gao, S.; Sui, Y.; Wei, F.; Qi, J.; Meng, Q.; Ren, Y.; He, Y. Dandelion-like nickel/cobalt metal-organic framework based electrode materials for high performance supercapacitors. *J. Colloid Interface Sci.* **2018**, *531*, 83–90. [[CrossRef](#)]
40. Xu, X.; Yang, J.; Hong, Y.; Wang, J. Nitrate Precursor Driven High Performance Ni/Co-MOF Nanosheets for Supercapacitors. *ACS Appl. Nano Mater.* **2022**, *5*, 8382–8392. [[CrossRef](#)]
41. Tang, X.R.; Li, N.; Pang, H. Metal-organic frameworks-derived metal phosphides for electrochemistry application. *Green Energy Environ.* **2022**, *7*, 636–661. [[CrossRef](#)]
42. Jiang, G.S.; Osman, S.; Senthil, R.A.; Sun, Y.Z.; Tan, X.; Pan, J.Q. Hierarchically porous carbon derived from magnesium-based metal-organic frameworks as advanced active material for supercapacitor. *J. Energy Storage* **2022**, *49*, 104071. [[CrossRef](#)]
43. Dai, Y.Y.; Liu, C.L.; Bai, Y.; Kong, Q.Q.; Pang, H. Framework materials for supercapacitors. *Nanotechnol. Rev.* **2022**, *11*, 1005–1046. [[CrossRef](#)]
44. Xu, S.J.; Dong, A.R.; Hu, Y.; Yang, Z.; Huang, S.M.; Qian, J.J. Multidimensional MOF-derived carbon nanomaterials for multifunctional applications. *J. Mater. Chem. A* **2023**, *11*, 9721–9747. [[CrossRef](#)]
45. Cao, Z.W.; Momen, R.; Tao, S.S.; Xiong, D.Y.; Song, Z.R.; Xiao, X.H.; Deng, W.T.; Hou, H.S.; Yasar, S.; Altin, S.; et al. Metal-Organic Framework Materials for Electrochemical Supercapacitors. *Nano-Micro Lett.* **2022**, *14*, 181. [[CrossRef](#)]
46. Kim, M.; Xin, R.J.; Earnshaw, J.; Tang, J.; Hill, J.P.; Ashok, A.; Nanjundan, A.K.; Kim, J.; Young, C.; Sugahara, Y.; et al. MOF-derived nanoporous carbons with diverse tunable nanoarchitectures. *Nat. Protoc.* **2022**, *17*, 2990–3027. [[CrossRef](#)]
47. Zhang, L.Y.; Wang, R.; Chai, W.C.; Ma, M.Y.; Li, L.K. Controllable Preparation of a N-Doped Hierarchical Porous Carbon Framework Derived from ZIF-8 for Highly Efficient Capacitive Deionization. *ACS Appl. Mater. Interfaces* **2023**, *15*, 48800–48809. [[CrossRef](#)]
48. Marpaung, F.; Kim, M.; Khan, J.H.; Konstantinov, K.; Yamauchi, Y.; Hossain, M.S.A.; Na, J.; Kim, J. Metal-Organic Framework (MOF)-Derived Nanoporous Carbon Materials. *Chem. Asian J.* **2019**, *14*, 1331–1343. [[CrossRef](#)]
49. Salunkhe, R.R.; Kaneti, Y.V.; Kim, J.; Kim, J.H.; Yamauchi, Y. Nanoarchitectures for Metal-Organic Framework-Derived Nanoporous Carbons toward Supercapacitor Applications. *Acc. Chem. Res.* **2016**, *49*, 2796–2806. [[CrossRef](#)]
50. Rajak, R.; Kumar, R.; Ansari, S.N.; Saraf, M.; Mobin, S.M. Recent highlights and future prospects on mixed-metal MOFs as emerging supercapacitor candidates. *Dalton Trans.* **2020**, *49*, 11792–11818. [[CrossRef](#)]
51. Kumar, N.; Wani, T.A.; Pathak, P.K.; Bera, A.; Salunkhe, R.R. Multifunctional nanoarchitected porous carbon for solar steam generation and supercapacitor applications. *Sustain. Energy Fuels* **2022**, *6*, 1762–1769. [[CrossRef](#)]
52. Khan, I.A.; Badshah, A.; Khan, I.; Zhao, D.; Nadeem, M.A. Soft-template carbonization approach of MOF-5 to mesoporous carbon nanospheres as excellent electrode materials for supercapacitor. *Micropor. Mesopor. Mat.* **2017**, *253*, 169–176. [[CrossRef](#)]
53. Li, Q.; Dai, Z.; Wu, J.; Liu, W.; Di, T.; Jiang, R.; Zheng, X.; Wang, W.; Ji, X.; Li, P.; et al. Fabrication of Ordered Macro-Microporous Single-Crystalline MOF and Its Derivative Carbon Material for Supercapacitor. *Adv. Energy Mater.* **2020**, *10*, 1903750. [[CrossRef](#)]
54. Huang, J.L.; Hao, F.; Zhang, X.H.; Chen, J.H. N-doped porous carbon sheets derived from ZIF-8: Preparation and their electrochemical capacitive properties. *J. Electroanal. Chem.* **2018**, *810*, 86–94. [[CrossRef](#)]
55. Gu, Y.; Miao, L.; Yin, Y.; Liu, M.; Gan, L.; Li, L. Highly N/O co-doped ultramicroporous carbons derived from nonporous metal-organic framework for high performance supercapacitors. *Chin. Chem. Lett.* **2021**, *32*, 1491–1496. [[CrossRef](#)]
56. Meng, F.; Fang, Z.; Li, Z.; Xu, W.; Wang, M.; Liu, Y.; Zhang, J.; Wang, W.; Zhao, D.; Guo, X. Porous Co₃O₄ materials prepared by solid-state thermolysis of a novel Co-MOF crystal and their superior energy storage performances for supercapacitors. *J. Mater. Chem. A* **2013**, *1*, 7235–7241. [[CrossRef](#)]
57. Zheng, S.; Li, Q.; Xue, H.; Pang, H.; Xu, Q. A highly alkaline-stable metal oxide@metal-organic framework composite for high-performance electrochemical energy storage. *Natl. Sci. Rev.* **2020**, *7*, 305–314. [[CrossRef](#)]
58. Wu, M.-S.; Xu, J.-X. Nickel-cobalt oxide nanocages derived from cobalt-organic frameworks as electrode materials for electrochemical energy storage with redox electrolyte. *Electrochim. Acta* **2019**, *319*, 31–40. [[CrossRef](#)]
59. Babu, S.K.; Raj, J.J.D.; Vijayakumar, T.; Gunasekaran, B. Experimental and DFT studies on spinel NiMn₂O₄ flower derived from bimetallic MOF as an efficient electrode for next-generation supercapacitor. *Colloids Surf. A Physicochem. Eng. Asp.* **2022**, *655*, 130244. [[CrossRef](#)]
60. Lim, G.J.H.; Liu, X.; Guan, C.; Wang, J. Co/Zn bimetallic oxides derived from metal organic frameworks for high performance electrochemical energy storage. *Electrochim. Acta* **2018**, *291*, 177–187. [[CrossRef](#)]
61. Acharya, D.; Pathak, I.; Dahal, B.; Lohani, P.C.; Bhattarai, R.M.; Muthurasu, A.; Kim, T.; Ko, T.H.; Chhetri, K.; Kim, H.Y. Immoderate nanoarchitectures of bimetallic MOF derived Ni-Fe-O/NPC on porous carbon nanofibers as freestanding electrode for asymmetric supercapacitors. *Carbon* **2023**, *201*, 12–23. [[CrossRef](#)]
62. Feng, Y.; Yao, J.F. Tailoring the structure and function of metal organic framework by chemical etching for diverse applications. *Coord. Chem. Rev.* **2022**, *470*, 214699. [[CrossRef](#)]
63. Shao, M.F.; Zhang, R.K.; Li, Z.H.; Wei, M.; Evans, D.G.; Duan, X. Layered double hydroxides toward electrochemical energy storage and conversion: Design, synthesis and applications. *Chem. Commun.* **2015**, *51*, 15880–15893. [[CrossRef](#)] [[PubMed](#)]
64. Cao, F.; Gan, M.; Ma, L.; Li, X.; Yan, F.; Ye, M.; Zhai, Y.; Zhou, Y. Hierarchical sheet-like Ni-Co layered double hydroxide derived from a MOF template for high-performance supercapacitors. *Synth. Met.* **2017**, *234*, 154–160. [[CrossRef](#)]

65. Huang, B.; Wang, W.; Pu, T.; Li, J.; Zhu, J.; Zhao, C.; Xie, L.; Chen, L. Two-dimensional porous (Co, Ni)-based monometallic hydroxides and bimetallic layered double hydroxides thin sheets with honeycomb-like nanostructure as positive electrode for high-performance hybrid supercapacitors. *J. Colloid Interface Sci.* **2018**, *532*, 630–640. [[CrossRef](#)]
66. Liu, Y.; Fu, N.; Zhang, G.; Xu, M.; Lu, W.; Zhou, L.; Huang, H. Design of Hierarchical Ni-Co@Ni-Co Layered Double Hydroxide Core-Shell Structured Nanotube Array for High-Performance Flexible All-Solid-State Battery-Type Supercapacitors. *Adv. Funct. Mater.* **2017**, *27*, 1605307. [[CrossRef](#)]
67. Wang, X.K.; Hao, C.; Zhang, J.S.; Ni, C.H.; Wang, X.H.; Shen, Y.T. Reasonable design and synthesis of nickel manganese sulfide nanoparticles derived from metal organic frameworks as electrode materials for supercapacitors. *J. Power Sources* **2022**, *539*, 231594. [[CrossRef](#)]
68. Li, S.S.; Yang, Y.; Hu, Z.B.; Li, S.; Ding, F.; Xiao, X.X.; Si, P.C.; Ulstrup, J. Hetero-structured NiS/CoS nanospheres embedded on N/S co-doped carbon nanocages with ultra-thin nanosheets for hybrid supercapacitors. *Electrochim. Acta* **2022**, *424*, 140604. [[CrossRef](#)]
69. Li, C.Y.; Wang, J.; Yan, Y.; Huo, P.W.; Wang, X.K. MOF-derived NiZnCo-P nano-array for asymmetric supercapacitor. *Chem. Eng. J.* **2022**, *446*, 137108. [[CrossRef](#)]
70. Sun, L.; Liu, Y.; Yan, M.; Yang, Q.J.; Liu, X.Y.; Shi, W.D. Lewis acid etched Ni_xCo_{1-x}Se₂ derived from ZIF-L on CoO nanowires for hybrid-supercapacitors. *Chem. Eng. J.* **2022**, *431*, 133472. [[CrossRef](#)]
71. Lu, X.F.; Xia, B.Y.; Zang, S.Q.; Lou, X.W. Metal-Organic Frameworks Based Electrocatalysts for the Oxygen Reduction Reaction. *Angew. Chem. Int. Ed.* **2020**, *59*, 4634–4650. [[CrossRef](#)]
72. Yang, B.L.; Li, B.J.; Xiang, Z.H. Advanced MOF-based electrode materials for supercapacitors and electrocatalytic oxygen reduction. *Nano Res.* **2022**, *16*, 1338–1361. [[CrossRef](#)]
73. Hosseinian, A.; Amjad, A.; Hosseinzadeh-Khanmiri, R.; Ghorbani-Kalhor, E.; Babazadeh, M.; Vessally, E. Nanocomposite of ZIF-67 metal-organic framework with reduced graphene oxide nanosheets for high-performance supercapacitor applications. *J. Mater. Sci. Mater. Electron.* **2017**, *28*, 18040–18048. [[CrossRef](#)]
74. Ramachandran, R.; Xuan, W.L.; Zhao, C.H.; Leng, X.H.; Sun, D.Z.; Luo, D.; Wang, F. Enhanced electrochemical properties of cerium metal-organic framework based composite electrodes for high-performance supercapacitor application. *RSC Adv.* **2018**, *8*, 3462–3469. [[CrossRef](#)] [[PubMed](#)]
75. Xu, S.; Liu, R.; Shi, X.; Ma, Y.; Hong, M.; Chen, X.; Wang, T.; Li, F.; Hu, N.; Yang, Z. A dual CoNi MOF nanosheet/nanotube assembled on carbon cloth for high performance hybrid supercapacitors. *Electrochim. Acta* **2020**, *342*, 136124. [[CrossRef](#)]
76. Ibrahim, I.; Zheng, S.; Foo, C.Y.; Huang, N.M.; Lim, H.N. Hierarchical nickel-based metal-organic framework/graphene oxide incorporated graphene nanoplatelet electrode with exceptional cycling stability for coin cell and pouch cell supercapacitors. *J. Energy Storage* **2021**, *43*, 103304. [[CrossRef](#)]
77. Chen, T.; Shen, T.; Wang, Y.; Yu, Z.; Zhang, W.; Zhang, Y.; Ouyang, Z.; Cai, Q.; Ji, Y.; Wang, S. In Situ Synthesis of Ni-BTC Metal-Organic Framework@Graphene Oxide Composites for High-Performance Supercapacitor Electrodes. *ACS Omega* **2023**, *8*, 10888–10898. [[CrossRef](#)]
78. Shao, L.; Wang, Q.; Ma, Z.; Ji, Z.; Wang, X.; Song, D.; Liu, Y.; Wang, N. A high-capacitance flexible solid-state supercapacitor based on polyaniline and Metal-Organic Framework (UiO-66) composites. *J. Power Sources* **2018**, *379*, 350–361. [[CrossRef](#)]
79. Xu, M.; Wang, X.; Ouyang, K.; Xu, Z. Two-Dimensional Metal-Organic Framework Nanosheets Grown on Carbon Fiber Paper Interwoven with Polyaniline as an Electrode for Supercapacitors. *Energy Fuels* **2021**, *35*, 19818–19826. [[CrossRef](#)]
80. Ramandi, S.; Entezari, M.H. Design of new, efficient, and suitable electrode material through interconnection of ZIF-67 by polyaniline nanotube on graphene flakes for supercapacitors. *J. Power Sources* **2022**, *538*, 231588. [[CrossRef](#)]
81. Hussain, I.; Iqbal, S.; Hussain, T.; Cheung, W.L.; Khan, S.A.; Zhou, J.; Ahmad, M.; Khan, S.A.; Lamiel, C.; Imran, M.; et al. Zn-Co-MOF on solution-free CuO nanowires for flexible hybrid energy storage devices. *Mater. Today Phys.* **2022**, *23*, 100655. [[CrossRef](#)]
82. Wang, L.; Jia, D.; Yue, L.; Zheng, K.; Zhang, A.; Jia, Q.; Liu, J. In Situ Fabrication of a Uniform Co-MOF Shell Coordinated with CoNiO₂ to Enhance the Energy Storage Capability of NiCo-LDH via Vapor-Phase Growth. *ACS Appl. Mater. Interfaces* **2020**, *12*, 47526–47538. [[CrossRef](#)] [[PubMed](#)]
83. Shi, X.; Deng, T.; Zhu, G. Vertically oriented Ni-MOF@Co(OH)₂ flakes towards enhanced hybrid supercapacitor performance. *J. Colloid Interf. Sci.* **2021**, *593*, 214–221. [[CrossRef](#)]
84. Lu, J.; Duan, H.; Zhang, Y.; Zhang, G.; Chen, Z.; Song, Y.; Zhu, R.; Pang, H. Directional Growth of Conductive Metal-Organic Framework Nanoarrays along [001] on Metal Hydroxides for Aqueous Asymmetric Supercapacitors. *ACS Appl. Mater. Interfaces* **2022**, *14*, 25878–25885. [[CrossRef](#)]
85. Shin, S.-J.; Gittins, J.W.; Balhatchet, C.J.; Walsh, A.; Forse, A.C. Metal-Organic Framework Supercapacitors: Challenges and Opportunities. *Adv. Funct. Mater.* **2023**, 2308497. [[CrossRef](#)]
86. Wang, W.J.; Chen, D.; Li, F.Y.; Xiao, X.; Xu, Q. Metal-organic framework-based materials as platforms for energy applications. *Chem* **2023**. [[CrossRef](#)]
87. Savariraj, A.D.; Raj, C.J.; Kale, A.M.; Kim, B.C. Road Map for In Situ Grown Binder-Free MOFs and Their Derivatives as Freestanding Electrodes for Supercapacitors. *Small* **2023**, *19*, 2207713. [[CrossRef](#)]
88. Xu, Y.X.; Li, Q.; Guo, X.T.; Zhang, S.T.; Li, W.T.; Pang, H. Metal organic frameworks and their composites for supercapacitor application. *J. Energy Storage* **2022**, *56*, 105819. [[CrossRef](#)]

89. Lokhande, P.E.; Kulkarni, S.; Chakrabarti, S.; Pathan, H.M.; Sindhu, M.; Kumar, D.; Singh, J.; Kumar, A.; Mishra, Y.K.; Toncu, D.C.; et al. The progress and roadmap of metal-organic frameworks for high-performance supercapacitors. *Coord. Chem. Rev.* **2022**, *473*, 214771. [[CrossRef](#)]
90. Zhang, H.H.; Gu, C.; Yao, M.S.; Kitagawa, S. Hybridization of Emerging Crystalline Porous Materials: Synthesis Dimensionality and Electrochemical Energy Storage Application. *Adv. Energy Mater.* **2022**, *12*, 2100321. [[CrossRef](#)]

Disclaimer/Publisher's Note: The statements, opinions and data contained in all publications are solely those of the individual author(s) and contributor(s) and not of MDPI and/or the editor(s). MDPI and/or the editor(s) disclaim responsibility for any injury to people or property resulting from any ideas, methods, instructions or products referred to in the content.